J Nanopart Res (2015) 17:144
DOI 10.1007/s11051-014-2746-y

RESEARCH PAPER

Imparting magnetic dipole heterogeneity to internalized iron oxide nanoparticles for microorganism swarm control

Paul Seung Soo Kim · Aaron Becker · Yan Ou · Anak Agung Julius · Min Jun Kim

Received: 28 July 2014 / Accepted: 10 November 2014 / Published online: 17 March 2015

Abstract *Tetrahymena pyriformis* is a single cell eukaryote that can be modified to respond to magnetic fields, a response called magnetotaxis. Naturally, this microorganism cannot respond to magnetic fields, but after modification using iron oxide nanoparticles, cells are magnetized and exhibit a constant magnetic dipole strength. In experiments, a rotating field is applied to cells using a two-dimensional approximate Helmholtz coil system. Using rotating magnetic fields, we characterize discrete cells' swarm swimming which is affected by several factors. The behavior of the cells under these fields is explained in detail. After the field is removed, relatively straight swimming is observed. We also generate increased heterogeneity within a population of cells to improve controllability of a swarm, which is explored in a cell model. By exploiting this straight swimming behavior, we propose a method to control discrete cells utilizing a single global magnetic input. Successful implementation of this swarm control method would enable teams of microrobots to perform a variety of in vitro microscale tasks impossible for single microrobots, such as pushing objects or simultaneous micromanipulation of discrete entities.

Keywords *Tetrahymena pyriformis* · Iron oxide nanoparticles · Magnetotaxis · Swarm control · Microrobot

Section(s) from this article were used in an earlier version presented at The International Conference on Ubiquitous Robots and Ambient Intelligence on October 30, 2013 (Kim et al. 2013), IEEE/RSJ International Conference on Intelligent Robots and Systems on November 13, 2013 (Becker et al. 2013), and reprinted, with permission (©2013 IEEE). This article presents a continuation.

Guest Editors: Leonardo Ricotti, Arianna Menciassi

This article is part of the topical collection on Nanotechnology in Biorobotic Systems

P. S. S. Kim · M. J. Kim (✉)
Department of Mechanical Engineering and Mechanics, Drexel University, Philadelphia, PA 19104, USA
e-mail: mkim@coe.drexel.edu

P. S. S. Kim
e-mail: psk25@drexel.edu

A. Becker
Department of Cardiovascular Surgery, Harvard University, Boston, MA 02115, USA
e-mail: aaron.becker@childrens.harvard.edu

Y. Ou · A. A. Julius
Department of Electrical, Computer, and Systems Engineering, Rensselaer Polytechnic Institute, Troy, NY 12180, USA
e-mail: ouy2@rpi.edu

A. A. Julius
e-mail: agung@rpi.edu

Introduction

Navigating microrobots through low Reynolds number fluids is a large hurdle in the field of robotics. In low Reynolds number environments, viscous forces dominate over inertial forces, and traditional methods of swimming will not work. Nature has developed methods to overcome viscous forces, such as cilia and flagella, through the use of non-reciprocal motion. Many research groups have looked to nature for inspiration and have developed such robotic microswimmers (Cheang et al. 2010; Dreyfus et al. 2005; Ghosh and Fischer 2009; Peyer et al. 2012a, b; Tottori et al. 2012; Weibel et al. 2005; Zhang et al. 2009, 2012, 2010). While these robots are capable of swimming in microfluidic environments, they are not able to be controlled to discrete points. We have developed a versatile microrobot platform: we focus on the well-studied (Kim et al. 2012b) protozoan *Tetrahymena pyriformis* (*T. pyriformis*). This microorganism makes a capable robot, as it has sensing abilities (sensory organelles), a powerful propulsion system (cilia that propels the cell up to 1,000 μm/s, or 20× its body length), is powered by its environment (takes nutrients in from its surroundings), and is cheap to produce en masse (cell culturing). Unlike other abiotic microswimmers, which require an external input to generate propulsion through rotation of the swimmers body, *T. pyriformis* is self propelled. As a result, this protozoan makes an ideal candidate for a microrobot.

To control microorganisms, specifically *T. pyriformis*, their behavioral response to stimuli is utilized. This response is known as a taxis. *T. pyriformis* has exhibited galvanotaxis (response to electric fields) (Brown et al. 1981; Kim et al. 2009; Ogawa et al. 2006), chemotaxis (chemical gradient) (Köhidai and Csaba 1998; Nam et al. 2007), and phototaxis (light) (Kim et al. 2009). While abiotic microrobot platforms exploit the specificity of engineered inorganic actuators, it is a great obstacle to imbed onboard sensing equipment analogous to the sensory organelles found in microorganisms. As a result, we are greatly interested in further characterizing *T. pyriformis* as a microrobot and organic actuator.

Magnetic fields are a great tool to control objects in the respect that they are able to be implemented globally without affecting other materials and demonstrate excellent material penetration. Magnetic fields have been used by researchers to control bacteria (Martel et al. 2009a, b, 2006) as well as abiotic microswimmers (Peyer et al. 2012a; Tottori et al. 2012). *T. pyriformis* has demonstrated that they can ingest particles up to 2.7 μm in diameter (Lavin et al. 1990). As a result, when seeding a culture tube containing *T. pyriformis* with iron oxide nanoparticles, we essentially create steerable robots that respond to magnetic fields after magnetization. In a low-frequency magnetic field, these swimmers will rotate in sync with the input frequency. We cannot directly control the amount of ingested iron oxide in cells, so naturally, after magnetization, there is some magnetic dipole strength heterogeneity, potentially allowing discrete control of these microrobots exploiting their step-out frequency, or the rotation field input frequency at which a magnetically responsive robot cannot follow. This has been investigated in magnet swimmers (Mahoney et al. 2014) but differs from our system because there is randomness in using microorganisms: motion and swimming parameters are less uniform and predictable with biological samples versus robots fabricated with precise methods. The global nature of magnetic fields makes discrete individual cell control difficult. Nevertheless, using a three-dimensional approximate Helmholtz system, a single *T. pyriformis* has been controlled and tracked in three dimensions (Kim et al. 2012a). Feedback algorithms and computer controlled magnetic fields have also been used to steer the cells (Kim et al. 2011; Ou et al. 2012).

Artificially magnetotactic *T. pyriformis* (AMT) aligns under a uniform magnetic field due to the torque generated. The response and time to align itself to a magnetic field are partially a function of the magnetic dipole strength, which is different for all cells. By exploiting the magnetic dipole strength heterogeneity, multiple cells may be able to be controlled using a single global magnetic field. In this paper, we explore the swimming behavior of AMT after nanoparticle modification under rotating magnetic fields in detail and propose a method for controlling a swarm of cells based on the results and model.

Materials and methods

Tetrahymena pyriformis culturing

T. pyriformis (Fig. 1, left) is cultured in a standard growth medium composed of 0.1 % w/v select yeast extract (Sigma Aldrich, St. Louis, MO) and 1 % w/v

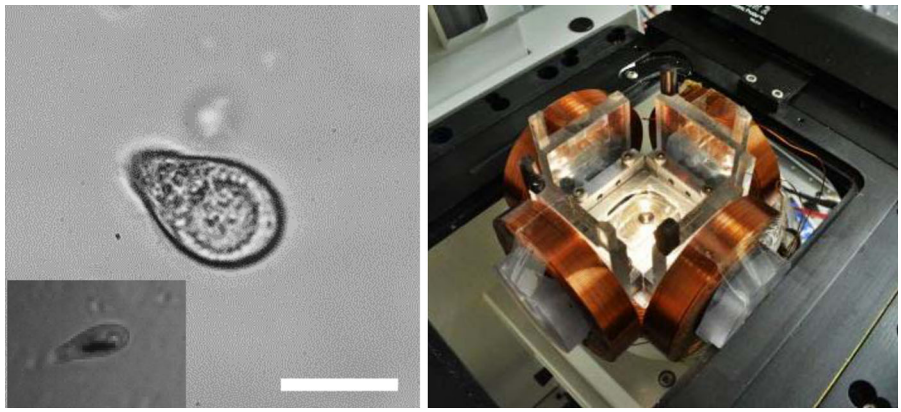

Fig. 1 (*left*) A single *Tetrahymena pyriformis* cell without any ingested iron oxide. (*inset*) A cell with internalized magnetized iron oxide. The *scale bars* are 25 μm. (*right*) Two pairs of approximate Helmholtz coils integrated into a microscope stage

tryptone (Sigma Aldrich, St. Louis, MO) in deionized water. Cell lines are maintained by transferring a small amount of cells into fresh medium weekly and incubated at 28 °C. Cells typically reach full saturation in 48 h (Köhidai and Csaba 1995). *T. pyriformis* is a pear-shaped cell that is 25 × 50 μm in size. It is a powerful swimmer, resulting from the arrays of ~600 cilia on its body. The cell utilizes two types of cilia: oral (for ingesting particles) and motile (arranged in arrays along the cells length used for swimming). The ciliary arrays run along the major axis of the cell and are on a slight axis. This slight angle results in a corkscrew motion during swimming.

Artificially magnetotactic *T. pyriformis*

Tetrahymena pyriformis does not normally respond to magnetic fields, but we have developed a method to make them artificially magnetotactic. 50-nm iron oxide particles (Sigma Aldrich, St. Louis, MO) are added to culture medium with *T. pyriformis* and then gently agitated to ensure uptake of the magnetite. The cells ingest these particles through their oral apparatus and enclose them in vesicles. In previous experiments, we have observed the internalized iron oxide in randomly scattered vesicles in the cell body, as well as their alignment after magnetization (Kim et al. 2010). The solution of cells is exposed to a permanent neodymium-iron-boron magnet (K&J Magnetics, Pipersville, PA). This magnetizes the ingested magnetite, as the particles should be fully saturated to react with the applied rotational magnetic fields. This exposure also separates the cells from the extraneous particles not consumed in the solution. After magnetization, the ingested iron oxide forms a rod-like shape inside the cell body along the cell's major axis due to the N–S poles. When a magnetic field is applied, the torque generated can be calculated using,

$$\tau = \boldsymbol{m} \times \boldsymbol{B} = mB \sin\theta \tag{1}$$

where τ, $\boldsymbol{m}$, and $\boldsymbol{B}$ represent the torque, magnetic moment, and the magnetic field, respectively. θ is the angle difference between the magnetic moment and the magnetic field. If the cell is orientated in a direction such that there is some nonzero value of θ, a torque will be generated, steering the cell to the direction of the magnetic field. Thus, when the cell is aligned with a magnetic field, no torque is generated, and the cell will continue to swim along this magnetic field.

AMT exhibits axial magnetotaxis. When cells are exposed to a permanent magnet after ingesting iron oxide, the internalized iron oxide becomes magnetized. However, the orientation of the dipole is random. That is, some cells will have a north to south polarity from the cell anterior to posterior, while other cells have the polarity reversed. This results in cells aligning themselves to any applied magnetic field, but they may swim in opposite directions. In experiments where a rotating magnetic field was implemented, the orientation of swimming AMT may differ in phase by about 180°. Experiments were conducted within an

hour after magnetization, during which we assume that the dipole strength remains constant. As *T. pyriformis* exhibits negative geotaxis, we have observed no surface effects whether they have or have not ingested iron oxide. In open channel observations, the cells swim freely throughout the vertical height of the fluid medium. Their swimming is unaffected in the presence of small aggregate magnetic particles, as they swim over and around them. As a result, we have assumed negligible surface effects for our models.

Experimental setup

Cells are placed in a microchannel to minimize any fluid flow and for ease of visualization. Microchannels are fabricated using SU-8 molds on silicon wafers made using standard photolithography techniques (Jo et al. 2000). An elastomer and curing agent mixture are poured onto silanized SU-8 molds. The resulting cured PDMS mold is then adhered onto glass slides using oxygen plasma treatment. Microchannels containing AMT are placed on the stage of an inverted LEICA DM IRB microscope. Images are captured for cells under constantly rotating magnetic fields with a Photron Fastcam SA3 using a 4× objective at 125 frames per second. An Edmund Optics 3112C CMOS camera is used to image cells with a 10× objective at 21.49 frames per second during characterization of cell motion when the a magnetic field is toggled. The final set of experiments is imaged with a Point Grey FL3-U3-13Y3M-C CMOS camera using a 4× objective at 30 frames per second while the frequency of the fields is varied.

At the center of the microscope, stage is an approximate 2D Helmholtz coil system. Two pairs of electromagnetics are placed on the x and y-axes to generate uniform magnetic field in 2 dimensions. Microchannels are placed on the center of the system, as shown in Fig. 1 (right). Because the magnetic field gradient (Fig. 2) is negligible, we assumed that there is no translation force from any non-uniform gradient and that only a torque is generated. LabVIEW is used to generate a constant rotational input at 6 rad/s through two power supplies (one for each axis). The position and orientation of cells are calculated using an image processing algorithm in MATLAB. Due to the axial magnetotactic nature of the cells, cells aligned on a magnetic field moving in opposite directions have a phase difference of 180°. The orientation of cells have been modified so all cells aligned to the magnetic field will have a θ value of 0 for better evaluation.

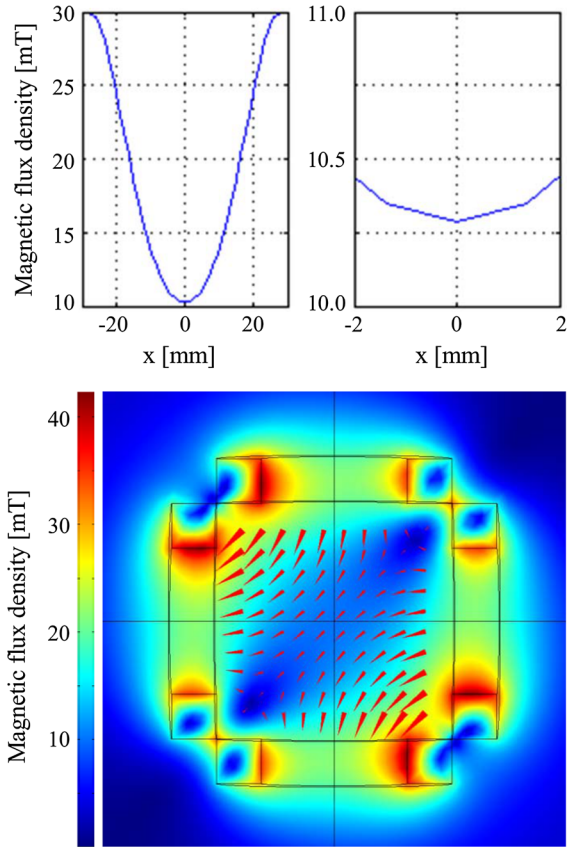

Fig. 2 Simulation of magnetic field strength of our 2D approximate Helmholtz coil system. (*top*) There is a negligible magnetic field gradient across an area of 2 mm, approximately the same size as the field of view of our experiments. These *plots* represent the field strength for both the x and y-axes. The uniformity of this field indicates that translation due to a magnetic field gradient is negligible. (*bottom*) The direction and magnitude of the magnetic fields are indicated by the *red* vectors. Vectors near the center are considered uniform for our system. This simulation was obtained using COMSOL Multiphysics. The area between the coils is 6.25 × 6.25 mm

Results and discussion

Constantly rotating magnetic fields

Cells are steered using magnetic fields. AMT is in a rotating magnetic field of 6 rad/s, seen in Fig. 3a. The difference between the magnetic field orientation and the cell's orientation is plotted in Fig. 3b. Without a magnetic field, the initial swimming trajectories of cells are random. Under these rotating magnetic fields, the cell trajectories are circular for low rotation speeds and complicated, perhaps hypotrochoidal, spiral patterns at high rotation speeds. Cells here were exposed to rotating

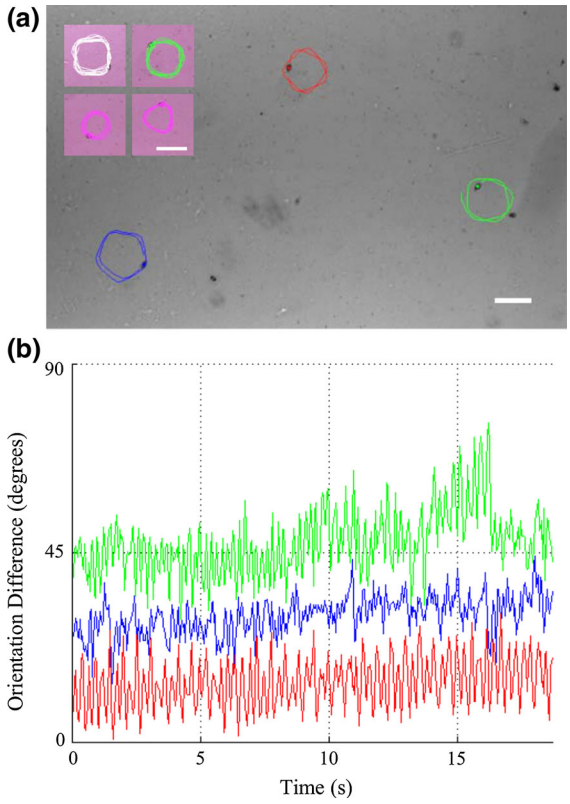

Fig. 3 **a** Three cells in a rotating magnetic field after 5 min. (*inset*) Trajectory of *red cell*, clockwise from top left, at $t = 1, 5, 10$, and 10.5 min. **b** The difference between the magnetic field orientation and the cell orientation is plotted here. The *colors* correspond to the top figure. The *scale bars* are 250 μm. (Color figure online)

magnetic fields for 5 min. There is a consistent difference between a cell's orientation and the orientation of the magnetic field. The mean difference is 20.6°, 36.6°, and 53.9° for the cells represented by the red, blue, and green plots, respectively.

The orientation difference observed here may be attributed to several factors. As *T. pyriformis* is biological organisms, there will be some variation between each cell, whether it is their speed, frequency of oscillation due to corkscrew motion, or size. Each cell also has a dipole strength which is a function of the magnetization of the particles as well as the amount of internalized magnetite. An AMT with a greater dipole strength or large amount of magnetized magnetite will show a more robust response to an applied magnetic field, aligning itself to the magnetic field faster than other AMT that may not have as high or as much dipole strength or internalized magnetite, respectively. Regardless, we see that the cell still manages to rotate with the same frequency as the rotating magnetic field.

There is also a slight upward trend in the orientation difference between all the cells. This trend is not consistent for these cells, as they have been swimming prior to this data capture for 5 min while matching the number of rotations and continue to do so for a remainder of 5 min. It is notable, however, that the cells trajectory and orientation difference will change over time. In (Fig. 3a, inset), the trajectories of a cell when exposed to magnetic fields (6 rad/s) for 1, 5, and 10 min is shown. The cell also decreased speed, evident from the decrease in radius. This decrease in speed may have resulted from the cell tiring or the slight temperature elevation of the chamber.

Characterization of cell motion during and after removal of rotating fields

Cells were placed in rotating magnetic fields (6 rad/s) for less than 10 s. Afterward, the magnetic field was

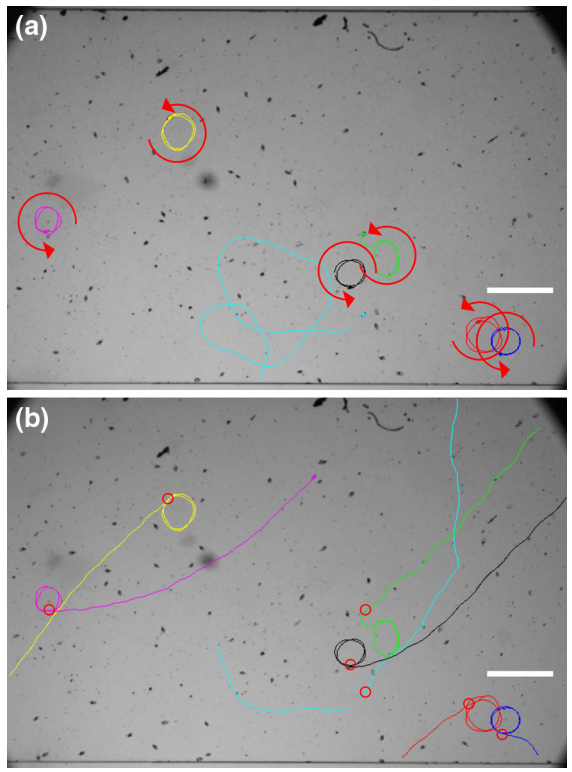

Fig. 4 **a** Trajectory of cells swimming under a 6 rad/s rotating magnetic field. **b** The same cells swimming in a straight direction after the rotating magnetic field is removed. *Red circles* indicate the last position of the cell prior to removing the magnetic field. The *scale bar* is 500 μm. (Color figure online)

switched off, and the swimming of the previously rotating cells was observed. Figure 4a shows cells swimming in circular trajectories while the magnetic field is on, and Fig. 4b shows cells after the field has been switched off. Circular trajectories varying in shape are observed for six different cells. In Fig. 5a, the black-dashed line in the plot represents the orientation of the field. Similar to the previous experiment of extended exposure to magnetic fields, there is a slight lag between the cell's orientation and direction of the magnetic field. The magnetic field is removed at 7.28 s, during which the orientation of the field is 31.3°. The power supplies were turned off to ensure that no magnetic field was present. The cells demonstrate typical corkscrew motion along a straight line. For 5 observed cells, the average difference between their orientation and the magnetic field was 11.6, 46.3, 46.6, 25.63, and 33.8° for the cells indicated by the red, blue, yellow, magenta, and black plots, respectively. When the field was removed, however, all demonstrated straight swimming, relative to their trajectory during rotation.

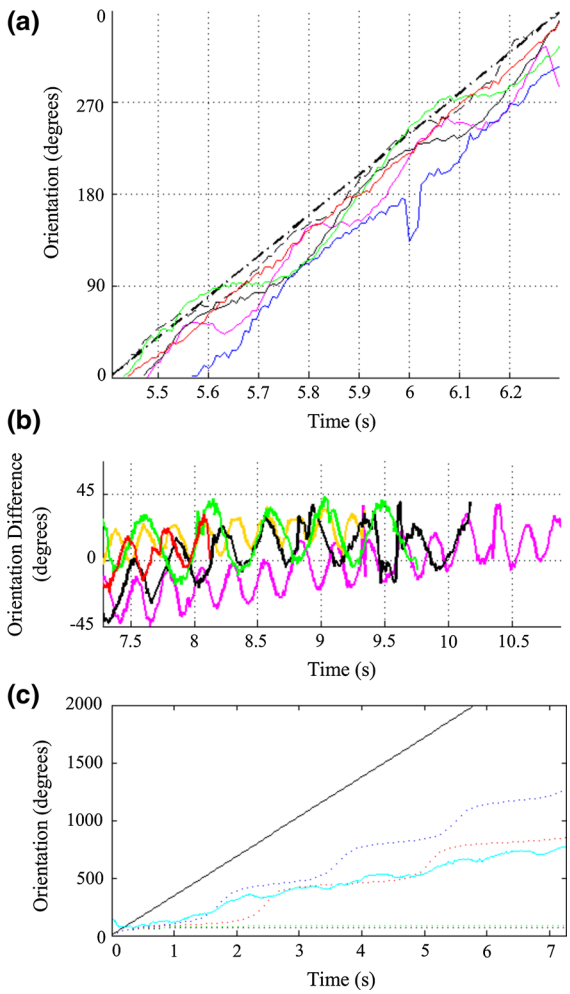

Fig. 5 **a** Cell orientation in a one period. The *dashed line* is the orientation of the magnetic field. Cells follow the magnetic field closely. The *colors* here match the cells in Fig. 4 except for the *dashed black line* (represented by *yellow trajectory*). *Red circles* represent kinks attributed to the cell's corkscrew motion. **b** The difference between the cell's orientation and the orientation of the magnetic field just prior to removal. Cells swim in relatively straight trajectories after removal of the magnetic field. **c** Cell with a high latency. Cells match simulation of cells that poorly follow the magnetic field. (Color figure online)

During the experiment, at times, a cell would overlap other cells, and our image processing was unable to identify each cell. As a result, there are some brief periods where a cell could not be tracked. Outlying data points in Fig. 5, such as the blue cell at 6 s, may be attributed to errors during centroid orientation calculations when another cell comes in close proximity or the cell swims over a distorted area (due to floating debris or interference in imaging).

In Fig. 5a, the cell exhibits a constant angular velocity and is able to rotate synchronously with magnetic fields, but there are periodic changes in slope possibly due to the cell's corkscrew swimming motion. The "kinks" for the blue, dashed black/yellow, magenta, and solid black cells during rotation are 2.0, 4.3, 4.2, and 2.4 Hz, respectively. The values for blue, dashed black/yellow, magenta, and solid black cells after the magnetic field is turned off are 2.1, 4.1, 3.8, and 2.7 Hz, respectively. The kinks for one cell are indicated by red circles in Fig. 5a.

Although most cells matched the rotation frequency of the magnetic field, there was one observed case where a cell could not match the frequency yet still exhibited a distinct influenced trajectory. Figure 5c shows a cyan cell which follows the magnetic field periodically. As previously mentioned, *T. pyriformis* exhibits a corkscrew motion when swimming due to the angled array of cilia along the length of the cell body. The cell appeared to rotate with the field when the direction of change and orientation of the cells oscillation were similar to that of the rotating magnetic field. During this point, it is likely that the cell experiences the greatest torque according to Eq. 1. This cell's magnetic moment may not have been as high as the other cells, resulting in the unique trajectory. The cell is plotted against a simulation (dashed lines) for cells with various

time constants for aligning themselves to the magnetic field. This cell closely follows with simulated cells that exhibit poor response to magnetic fields, indicating the accuracy and potential of our model for swarm control. The cell also turns slightly after the removal of the field. This can be attributed to normal cell motion, as the biological nature of cells is inherently random, although rarely observed during experiments. The slight curve to the pink cells motion can also be attributed to the cell's innate swimming behavior, as we have previously observed cells directly from a new culture to swim in slight arcs. The next set of experiments imitated the low magnetization of this cell in various frequencies.

Increasing magnetic dipole heterogeneity of cells in a population

All but one cell in the previous experiments had a phase lag of less than 90 degrees. Their departing orientation after the removal of magnetic fields was different but was all within a small range. Ideally, for swarm control, multiple cells should exhibit a large range of heterogeneity in their response rate for a single global input. Understanding how $\boldsymbol{m}$, the magnetic dipole strength, affects the response rate, and phase lag is key.

We know that AMT is able to swim due to the torque caused by the magnetic field. We can also calculate the torque using Eq. (1). AMT can be discretely controlled using a global input because of the inhomogeneity of the magnetic dipole strength of each cell, mainly. The magnetic dipole strength and the cells response are affected by several factors: (1) the amount of ingested magnetite, (2) the strength of the permanent magnet used to create these magnetic dipoles, and (3) the strength of the magnetic field. (1) is difficult to regulate and (3) cannot increase inhomogeneity of $\boldsymbol{m}$. A population of AMT will have a similar $\boldsymbol{m}$, seeded in an iron oxide nanoparticle solution for equal periods and magnetized with the same strength permanent magnet. As a result, higher frequencies would be necessary since lower frequencies would result in similar limit cycles. However, in preliminary experiments, we found that using rotating magnetic field that is high in frequency, such as 20 Hz, can affect the swimming of the cell after the fields are removed (cells do not exhibit corkscrew turning or rotation while swimming, reduction in speed), so for experiments outlined in this paper, we limited the frequency to 3 Hz. Therefore, it is desirable to vary $\boldsymbol{m}$ and increase the inhomogeneity of a population of cells by magnetizing cells with various strength magnets. We previously observed phase lag and a minority of cells unable to match the input frequency of the magnetic field, but in most cases, this can be attributed to a very small amount of ingested iron oxide. Using the method of various magnetization strengths, we can increase the consistency of the heterogeneity of the response rate.

Cells were separated after seeding the culture medium with iron oxide nanoparticles into two separated 1.5 mL volumes (Fig. 6). Each volume was magnetized with magnets with difference surface field strengths: 821 gauss and 1601 gauss. Equal parts from each volume were then placed into a PDMS microchannel. For these cells, they were exposed to a 3 Hz (6π rad/s) clockwise rotating field for 5 min, followed by a high/low frequency toggling and then complete removal of a field. Figure 7 illustrates the trajectory of two cells, each from the two discretely magnetized volumes of cells over a period of 28.37 s. From 0–0.67 s, the field frequency was 3 Hz. After, the field is toggled to 1 Hz (2π rad/s). At 18 s, the field was toggled back to 3 Hz and then removed at 24.67 s. Figure 7a illustrates the trajectory of the cells from 0–4 s. The trajectory of the initial 3 Hz field can be recognized by the smaller radius of cell A (thin green trajectory), which has a much stronger magnetic dipole strength than cell B (thick blue trajectory). The small red circles indicate the position of the cells when the field is toggled, and the solid circle represents the starting position of the cell. The orientation difference is also plotted in Fig. 8a. In this frequency, cells A and B maintain an average phase lag of 3.94° and 23.06°, respectively. Figure 7b shows the trajectory cells after the field is toggled from 1 Hz to 3 Hz. Cell A exhibits a steady phase lag of 27.03°. Cell B exceeds the step-out frequency, when the phase lag increases without bounds, and its trajectory is hypotrochoidal. Cell B's growing phase lag can be seen in Fig. 8b. Cell A maintains a phase lag of 27.03°, compared to 3.94° in a 1 Hz field.

At 24.67 s, the magnetic field is turned off. When a magnetic field is removed, the cells swim in the direction that they were in prior to the field's removal. The inset of Fig. 8b is the orientation

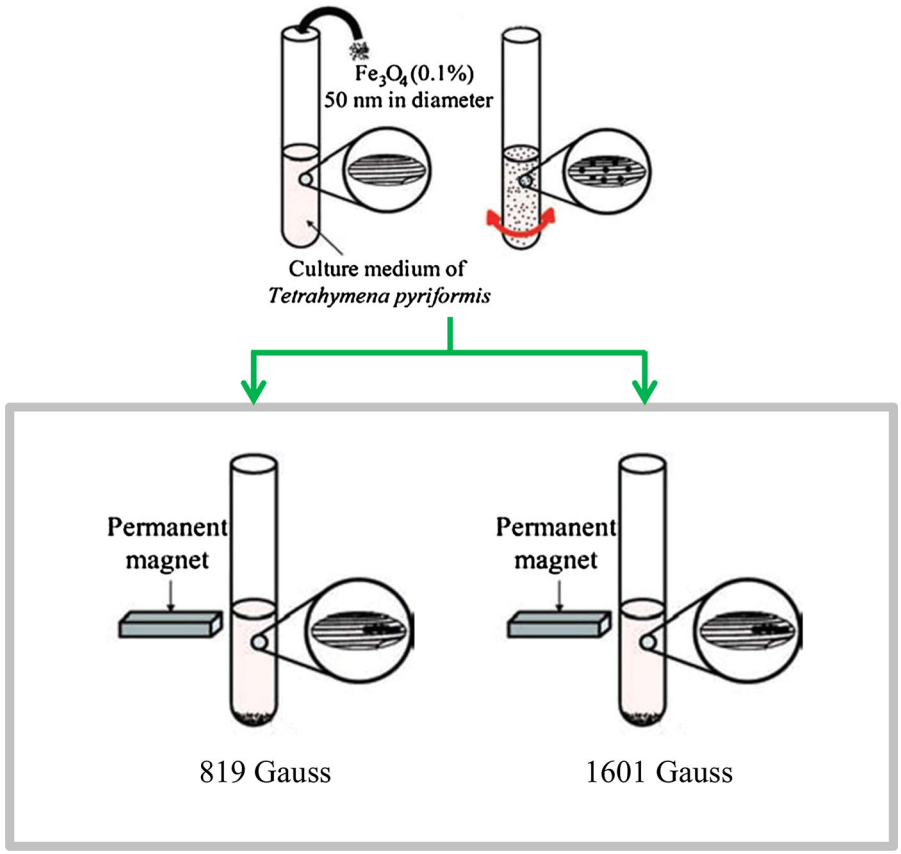

Fig. 6 Artificially magnetotactic *Tetrahymena pyriformis* is created by adding iron oxide nanoparticles into culture medium with cells. The cells are left for several minutes to ensure uptake of the iron oxide. Cells are then divided up into two separate volumes. One set of cells is magnetized with a permanent magnet with a surface field strength of 819 gauss and the other with a permanent magnet with a surface field strength of 1,601 gauss. Equal parts of each magnetized set of cells are then placed in a microfluidic chamber and into a magnetic field controller for experiments

difference between the cell and the last input of the magnetic field after the applied voltage to the controller was 0. The final orientation of the magnetic field was 117°. Cell A maintains an average orientation of 141.47° after the field's removal. This is only a difference of 2.56° between the cells straight swimming orientation and the cell's phase lag during in the 3 Hz rotational field. After removal of the field, cell B originally had a heading of 17.97°. After 3.7 s, its heading is 331.46°, which is an average angular velocity of −12.57°/second. AMT, like normal *T. pyriformis*, exhibits corkscrew swimming due to the angle of the axial array of motile cilia on its body. Looking at cell B's orientation change between each frame, there seems to be a bias toward counterclockwise movement, resulting in a net counterclockwise movement. This may be attributed to minute residual fields from any noise present in the system or nearby ferric objects. This biased swimming, however, is negligible for any future feedback control as cells would be under the influence of a magnetic field more often than not.

Modeling

For modeling, we will work with a simplified 2D approach that ignores the effects of gravity and collisions. Both are well documented, and their effects on control strategies warrant further study. Gravity alone would not make the system ensemble controllable, but boundary effects may. Disturbances from robot–robot interactions are also ignored and may be significant. Extending the model to 3D requires additional states and motion primitives, similar to those used for 2D. Bistable configurations were considered for our model, as they are observed in magnetic helical swimmers and other nanostructures (Ghosh et al. 2013, 2012; Morozov and Leshansky 2014). In these cases, at high frequencies, a precession angle may form, and the magnetic moment is not planar with the rotating fields, and, for our system, would indicate that there would be translation in the z-axis as the cell body aligns to the aggregated iron oxide. We have verified in experimental methods that our cells remain planar, and that no precession angles

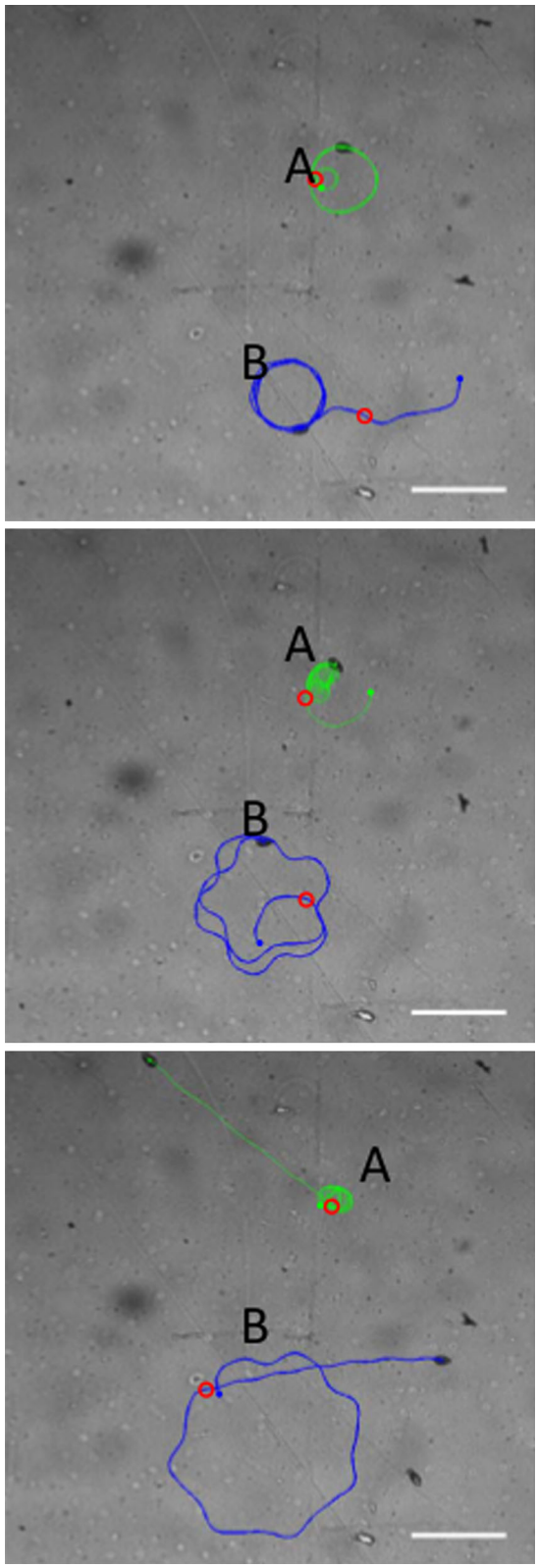

◀**Fig. 7** Trajectory of cells during various frequency toggling. Each pane represents 4 s when the field is switched from (*top*) 3 to 1 Hz, (*center*) 1 to 3 Hz, and (*bottom*) 3 to 0 Hz. Starting positions of cell A (*thin green line*) and cell B (*thick blue line*) are indicated with *solid circles*; magnetic field frequency toggling is indicated by hollow *red circles*. *Scale bar* is 250 μm. (Color figure online)

and bistable configurations exist in our system for our range of inputs.

Let the dynamic model for the *i*th cell shown in Fig. 9, with turning time constant a_i, be

$$\begin{bmatrix} \dot{x}_i \\ \dot{y}_i \\ \dot{\theta}_i \end{bmatrix} = \begin{bmatrix} v_i \cos\theta_i \\ v_i \sin\theta_i \\ Ma_i \sin(\psi - \theta_i) \end{bmatrix} \tag{2}$$

Here the x_i, y_i are Cartesian coordinates, θ_i is the orientation of the cell, ψ is the orientation of the magnetic field, and v_i is the swimming speed of the cell. The cell is pulled to orient along the magnetic field ψ by a magnetic field of magnitude M, and the rate of this alignment is given by the parameter a_i. We assume that the relationship is first order for some range about 0 and thus can be modeled as an ideal torsional spring. As long as the magnetic field is on, in steady-state, a large group of magnetized cells will share the same orientation. No steady-state dispersion in orientation is possible when a magnetic field is present. It may be possible to command a change in ψ, quickly turn off the magnetic field, and get a distribution of orientations parameterized by a, but this dispersion will vanish when the magnetic field is replaced. The nonlinear term $\sin(\psi - \theta_i)$ is due to the periodicity of the magnetic torque. For small $|\theta - \psi|$, we can use the small-angle approximation $(\theta - \psi)$.

Constantly rotating magnetic field

To make multiple cells controllable by the same magnetic field, we must exploit heterogeneity in turning rate. One method is by using a constantly rotating magnetic field $(t) = ft$, where $f \in \mathrm{R}^+$ is the frequency of rotation. For $f < Ma$, the cells will reach a steady-state phase lag as they attempt to align with the field. At steady-state the cells are turning at the same speed as the magnetic field

$$\begin{aligned} \dot{\theta}_i &= Ma_i \sin(\theta_i(t) - \psi(t)) \\ f &= Ma_i \sin(\theta_i(t) - ft) \\ \sin^{-1}\left(\frac{f}{Ma_i}\right) &= \theta_i(t) - ft \end{aligned} \tag{3}$$

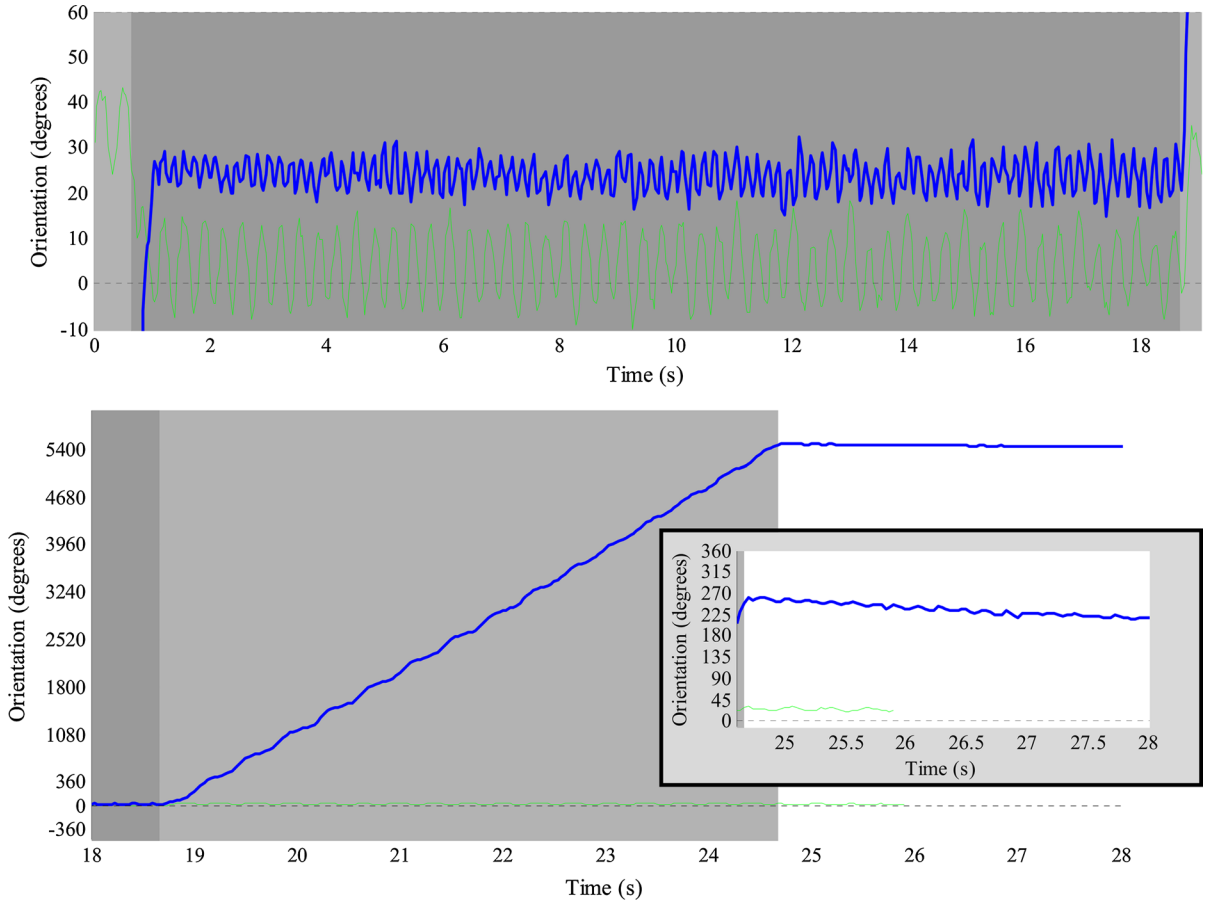

Fig. 8 Cells are under a field toggled between 3 and 1 Hz, following the removal of the field. The *colors* (thickness for *grayscale*) correspond to the trajectories shown in Fig. 7. Field frequency is indicated by the region shading: the *lighter region* represents a frequency of 3 Hz, and the *darker region* represents a field frequency of 1 Hz. The average orientation difference was 3.94 and 23.06° for the strong (*thin green*) and weakly (*thick blue*) magnetized cell, respectively. The *bottom plot* represents the orientation difference between the magnetic field and cells orientation. The strong magnetized cell maintained an average orientation difference of 27.03°. The weak magnetized cell could not keep up with the magnetic field, and its orientation difference increased linearly. *Inset* shows orientation difference of cells and the last direction of the magnetic field after removal of magnetic field. (Color figure online)

This steady-state phase lag is shown in Fig. 10. The quantity $\frac{f}{Ma_i}$ is the *step-out frequency*, after which the phase lag grows without bound. This growth is approximately linear for $>1.5a$, as shown in Fig. 11. The effective period for the cell is

$$T_i = \begin{cases} \dfrac{2\pi}{f}, & f < Ma_i \\ \approx 12.9f(Ma_i)^{-2} - 2.3(Ma_i)^{-1}, & else \end{cases} \quad (4)$$

We can also compute the effective radius of the limit cycle the cell follows. For $f < a$, the cell completes a cycle every $2\pi/f$ seconds, and the radius is therefore v/f. Past the step-out frequency, the cells turn in periodic orbits similar to the hypotrochoids and epitrochoids produced by a Spirograph® toy. Representative limit cycles are shown in Fig. 12. The radius of rotation is

$$r_i = \begin{cases} \dfrac{v_i}{f}, & f < Ma_i \\ \approx 1.45f(Ma_i)^{-2} - 0.3(Ma_i)^{-1}, & else \end{cases}$$

Arbitrary orientations

If we could control the orientation of each cell independently, the cells could swim directly to the

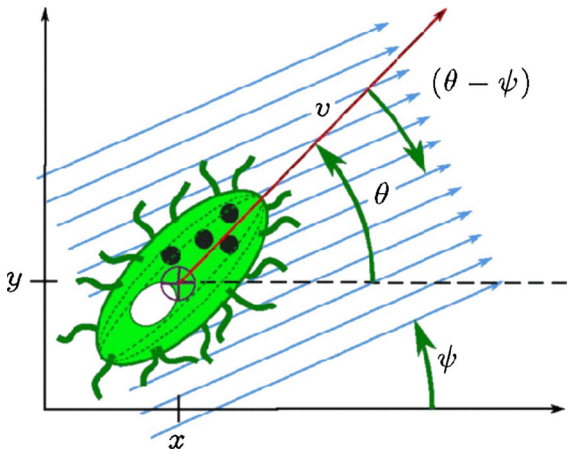

Fig. 9 Kinematic model of a magnetized *T. pyriformis* cell. The magnetic field exerts torque $Ma_i \sin(\psi - \theta_i)$ to align the cell axis θ with the field ψ

goal. Figure 13 shows two cells with different a parameters. If the rotation frequency f and the a values are coprime, the range of possible θ_1 and θ_2 values span $[0, 2\pi] \times [0, 2\pi]$. By increasing f, we can control the density that we sample these angles. The left side of Fig. 13 shows that the time required to span $[0, 2\pi] \times [0, 2\pi]$ increases with f.

Straight-line swimming

By turning the magnetic field off, the cell dynamic model simplifies to

$$\begin{bmatrix} \dot{x}_i \\ \dot{y}_i \\ \dot{\theta}_i \end{bmatrix} = \begin{bmatrix} v_i \cos\theta_i \\ v_i \sin\theta_i \\ 0 \end{bmatrix} \tag{5}$$

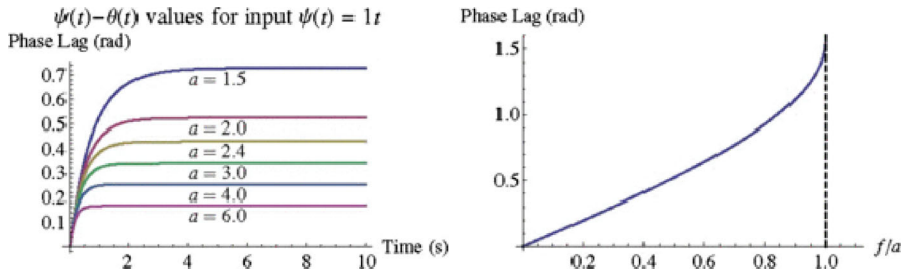

Fig. 10 A cell modeled by (2), under a constantly rotating magnetic field $\psi(t) = ft$ will reach a steady-state phase lag of $\sin^{-1}\left(\frac{f}{a}\right)$ radians. $f = Ma$ is the *step-out frequency*, after which the phase lag grows without bound. This growth is approximately linear

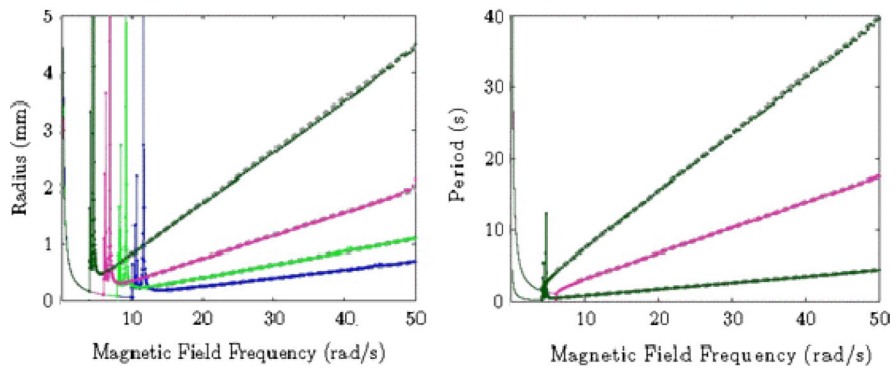

Fig. 11 As the magnetic field frequency f increases the radius, the cell swims in and the period of rotation decrease in a reciprocal relationship until a, the cutoff frequency. The radius values are erratic from a to $1.5a$ but, after $1.5a$, are linear in a^2 (a linear-fit line is in *dashed gray*: $r = 1.45\left(\frac{f}{a^2}\right) - \frac{0.3}{a}$, $T = 12.9\left(\frac{f}{a^2}\right) - \frac{2.3}{a}$. Shown are $a = [4, 6, 8, 10]$

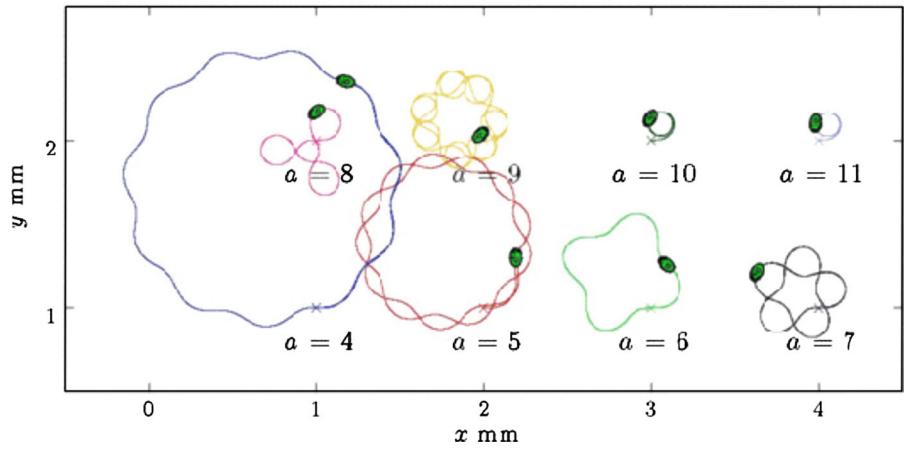

Fig. 12 Limit cycles for 8 cells simulated for 10 s with different values at $f = 10\,\text{rad/s}$. MATLAB code available online www.tinyurl.com/kx7rdmh

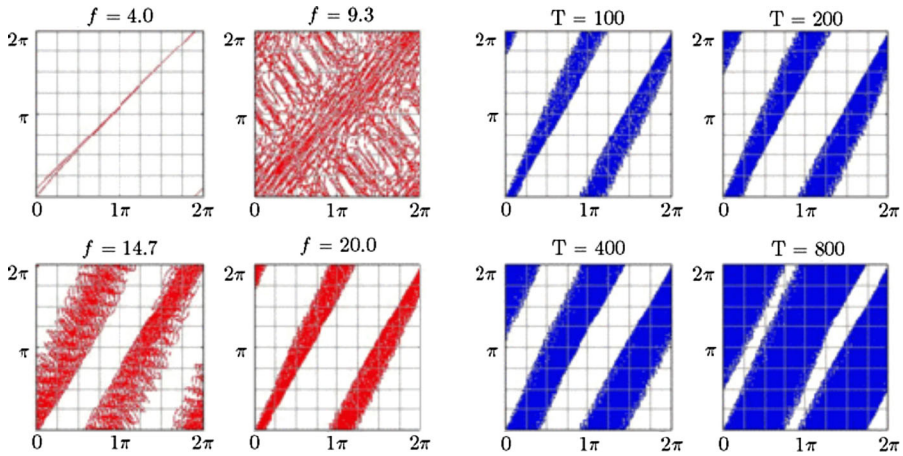

Fig. 13 Shown are the heading angles for two cells with $a = \{5, 7\}$. The x axis is θ_1, y axis θ_2. (*left*) Simulation for 100 s at increasing rotation frequencies f of the external magnetic field. If f and the a values are coprimes, the possible angular values span $[0, 2\pi] \times [0, 2\pi]$. (*right*) Rotation frequency of the external magnetic field $f = 20\,\text{rad/s}$ simulated for increasing amounts of time. As time increases, the set of possible angular value pairs becomes dense

Without an external magnetic field, the cells swim straight in the direction that they were headed when the magnetic field was last on. If we store the orientation of the magnetic field when the magnetic field is turned off at time t_a as $\psi_a = ft_a$, then when we turn the field back on at time t_b, we can resume where we last stopped $\psi(t) = \psi_a + f(t - t_b)$, and the cells will continue their limit-cycle behavior, but the center of rotation will be translated$v_i(t_b - t_b)$ along the vector $\theta_i\,(t_a)$.

System identification

To choose the optimal frequency of the rotation magnetic field requires knowing the a values for the set of cells, we want to control. We employ the method of least squares to determine the a_i values. First we discretize the continuous plant model (Eq. 2)

$$\begin{bmatrix} x_i(k+1) \\ y_i(k+1) \\ \theta_i(k+1) \end{bmatrix} = \begin{bmatrix} v_i \Delta T \cos\theta_i(k) \\ v_i \Delta T \sin\theta_i(k) \\ M\alpha_i \sin(\psi(k) - \theta_i(k)) \end{bmatrix} \tag{6}$$

where ΔT is the sampling time and $\alpha_i = a_i \Delta T$.

To identify the α_i parameter for each cell, we record position and orientation measurements under a constantly rotating magnetic field. We record the discrete-time cell orientation information as $\theta_i(0)$, $\theta_i(1)$, …, $\theta_i(k)$,…,$\theta_i(n)$, and the magnetic field orientation as $\psi(0)$, $\psi(1)$, …, $\psi(k)$,…,$\psi(n)$. The following equation is derived from Eq. 6.

$$\begin{bmatrix} \theta_i(1)-\theta_i(0) \\ \theta_i(2)-\theta_i(1) \\ \vdots \\ \theta_i(k)-\theta_i(k-1) \\ \vdots \\ \theta_i(n)-\theta_i(n-1) \end{bmatrix} = \begin{bmatrix} sin(\psi(0)-\theta_i(0)) \\ sin(\psi(1)-\theta_i(1)) \\ \vdots \\ sin(\psi(k-1)-\theta_i(k-1)) \\ \vdots \\ sin(\psi(n-1)-\theta_i(n-1)) \end{bmatrix} \cdot \alpha_i \tag{7}$$

We rewrite this equation as $Y = \Phi\alpha_i$. Then, using the method of least squares, the parameter set with the best fit to the data is given by $\hat{\alpha}_i = \Phi^{\dagger}Y$,, where $\Phi^{\dagger} = (\Phi^T\Phi)^{-1}\Phi^T$. is the pseudoinverse of Φ. The cell's a_i value is derived as $a_i = \frac{\alpha_i}{\Delta T}$.

The a_i value can also be measured directly by inverting Eq. (3). If the frequency of the rotation magnetic field is below the step-out frequency, the cells turn in a circle with a constant phase lag $\theta_{i,lag}$. The turning-rate parameter is then $a_i = -f/sin(\theta_{i,lag})$.

Swarm control

Once a rotating magnetic field has been removed, cells continue to swim straight, although in slightly different directions. This difference in orientation may be used to control swarms of cells to congregate or s—teer them to arbitrary positions. Using a combination of rotating and straight swimming (swimming in the presence and absence of a rotating magnetic field), a scenario such as that illustrated in Fig. 14 may be accomplished with many cells. A system can implement a toggling magnetic field to characterize cells and then calculate the most efficient path for goals.

Our control input consists of an alternating sequence of ORBIT and SWIM-STRAIGHT modes. The oscillation frequency f of the magnetic field is constant for every ORBIT mode. At the beginning of each ORBIT mode, the phase of the magnetic oscillation is resumed from the previous ORBIT mode. During the first ORBIT mode, we identify the centers of rotation ($x_{c,i}$, $y_{c,i}$) of each cell by recording the cell positions for at least one period, calculated by Eq. 4, and computing

$$\begin{aligned} x_{c,i}(t) &= max(x_i(t-T:t)) - min(x_i(t-T:t)) \\ y_{c,i}(t) &= max(y_i(t-T:t)) - min(y_i(t-T:t)) \end{aligned} \tag{8}$$

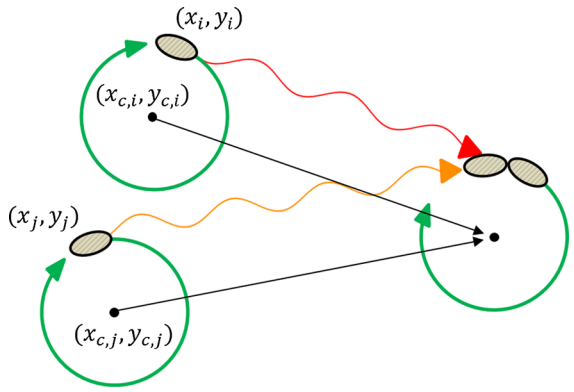

Fig. 14 A scenario for swarm control using a combination of straight and rotating swimming to direct two cells to the same orbit using a global input. In STRAIGHT-SWIM modes, the center of the cell's rotation changes and in ORBIT modes, the cell's center remains constant. The heading direction of cells will vary after the movement mode is toggled from ORBIT to STRAIGHT-SWIM. Models of the cell and a feedback algorithm could potentially be implemented in a vision-based tracking system to control two or more cells

The center of rotation of each cell translates along with the cell during each SWIM-STRAIGHT mode (see Fig. 14). Control laws were designed from a control-Lyapunov function and investigated in Becker et al. (2013).

Conclusion

In this paper, we have utilized iron oxide nanoparticles to impart a response to magnetic fields in a single cell eukaryote *Tetrahymena pyriformis*. We characterized the swarming motion of these artificially magnetotactic *T. pyriformis* in the presence and removal of rotating magnetic fields. We found that each cell's unique magnetic moment and other innate differences result in a phase lag when following a rotating magnetic field. In a constant rotating field, cells demonstrated a relatively even lag behind the applied fields. This phase lag in can also be seen when the magnetic fields are removed: cells swim straightly but in various orientations equal to the last directional input for the magnetic field minus the individual cell's phase lag.

The model that we have developed can calculate the magnetic response rates of each cell. This parameter enables us to predict the motion of the cell in a rotating

magnetic field that is toggled on and off. In a population with a near-homogenous magnetic dipole, cells would exhibit very similar phase lags and step-out frequencies, making discrete control of individual cells more difficult and decreasing the controllability of the system. Magnetizing discrete populations of cells with various strength magnets are the best solution to increasing the heterogeneity of the magnetic dipole strength, resulting in greater controllability of cells, as the range of orientations after a magnetic field's removal for two cells is greater. By exploiting rotating and straight swimming, a swarm control method using rotating fields may be implemented to control a swarm of cells, according to the motion models developed above. Various control laws to take advantage of these models can be taken from Becker et al. (2013). Hardware experiments with multiple cells are promising. Discrete control of multiple cells will enable us to perform complex microassembly and micromanipulation tasks such as pushing a single large object or multiple objects simultaneously.

Acknowledgments This work was supported by the National Science Foundation under CMMI 1000255, CMMI 1000284, and by ARO W911F-11-1-0490.

References

Becker A, Yan O, Kim P, Min Jun K, Julius A Feedback control of many magnetized: Tetrahymena pyriformis cells by exploiting phase inhomogeneity. In: Intelligent Robots and Systems (IROS), 2013 IEEE/RSJ International Conference on, 3–7 Nov. 2013 2013. pp 3317-3323. doi:10.1109/IROS.2013.6696828

Brown ID, Connolly JG, Kerkut G (1981) Galvanotaxic response of Tetrahymena vorax. Comp Biochem Physiol Part C: Comp Pharmacol 69:281–291

Cheang UK, Roy D, Lee JH, Kim MJ (2010) Fabrication and magnetic control of bacteria-inspired robotic microswimmers. Appl Phys Lett 97: 213704

Dreyfus R, Baudry J, Roper ML, Fermigier M, Stone HA, Bibette J (2005) Microsc Artif Swim. Nature 437:862–865

Ghosh A, Fischer P (2009) Controlled propulsion of artificial magnetic nanostructured propellers. Nano Lett 9:2243–2245. doi:10.1021/nl900186w

Ghosh A, Paria D, Singh HJ, Venugopalan PL, Ghosh A (2012) Dynamical configurations and bistability of helical nanostructures under external torque. Phys Rev E 86:031401

Ghosh A, Mandal P, Karmakar S, Ghosh A (2013) Analytical theory and stability analysis of an elongated nanoscale object under external torque. Phys Chem Chem Phys 15:10817–10823

Jo BH, Van Lerberghe LM, Motsegood KM, Beebe DJ (2000) Three-dimensional micro-channel fabrication in polydimethylsiloxane (PDMS) elastomer. J Microelectromech Syst 9:76–81. doi:10.1109/84.825780

Kim DH, Casale D, Kőhidai L, Kim MJ (2009) Galvanotactic and phototactic control of Tetrahymena pyriformis as a microfluidic workhorse. Appl Phys Lett 94:163901

Kim DH, Cheang UK, Kőhidai L, Byun D, Kim MJ (2010) Artificial magnetotactic motion control of Tetrahymena pyriformis using ferromagnetic nanoparticles: a tool for fabrication of microbiorobots. Appl Phys Lett 97:173702

Kim DH, Brigandi SE, Kim P, Byun D, Kim MJ (2011) Characterization of deciliation-regeneration process of tetrahymena pyriformis for cellular robot fabrication. J Bionic Eng 8:273–279

Kim DH, Kim PSS, Agung Julius AA, Kim MJ (2012a) Three-dimensional control of Tetrahymena pyriformis using artificial magnetotaxis. Appl Phys Lett 100: 053702

Kim M, Steager E, Julius AA, Agung J (2012b) Microbiorobotics: biologically inspired microscale robotic systems. William Andrew

Kim PSS, Becker A, Yan O, Julius AA, Min Jun K (2013) Swarm control of cell-based microrobots using a single global magnetic field. In: Ubiquitous Robots and Ambient Intelligence (URAI), 2013. 10th International Conference on, Oct 30 2013–Nov 2 2013. pp 21–26. doi:10.1109/URAI.2013.6677461

Köhidai L, Csaba G (1995) Effects of the mammalian vasoconstrictor the immunocytological detection of endogenous activity. Comp Biochem Physiol C: Pharmacol Toxicol Endocrinol 111:311–316. doi:10.1016/0742-8413(95)00055-S

Köhidai L, Csaba G (1998) Chemotaxis and chemotactic selection induced with cytokines (IL-8, Rantes and TNF-α) in the unicellular Tetrahymena pyriformis. Cytokine 10:481–486

Lavin DP, Hatzis C, Srienc F, Fredrickson A (1990) Size effects on the uptake of particles by populations of Tetrahymena pyriformis cells. J Protozool 37:157–163

Mahoney AW, Nelson ND, Peyer KE, Nelson BJ, Abbott JJ (2014) Behavior of rotating magnetic microrobots above the step-out frequency with application to control of multi-microrobot systems. Appl Phys Lett 104: 144101

Martel S, Tremblay CC, Ngakeng S, Langlois G (2006) Controlled manipulation and actuation of micro-objects with magnetotactic bacteria. Appl Phys Lett 89:233904. doi:10.1063/1.2402221 233904

Martel S et al (2009a) MRI-based medical nanorobotic platform for the control of magnetic nanoparticles and flagellated bacteria for target interventions in human capillaries. Int J Robot Res 28:1169–1182. doi:10.1177/0278364908104855

Martel S, Mohammadi M, Felfoul O, Lu Z, Pouponneau P (2009b) Flagellated magnetotactic bacteria as controlled MRI-trackable propulsion and steering systems for medical nanorobots operating in the human microvasculature. Int J Robot Res 28:571–582. doi:10.1177/0278364908100924

Morozov KI, Leshansky AM (2014) The chiral magnetic nanomotors. Nanoscale 6:1580–1588

Nam S-W, Van Noort D, Yang Y, Park S (2007) A biological sensor platform using a pneumatic-valve controlled

microfluidic device containing Tetrahymena pyriformis. Lab Chip 7:638–640. doi:10.1039/b617357h

Ogawa N, Oku H, Hashimoto K, Ishikawa M (2006) A physical model for galvanotaxis of Paramecium cell. J Theor Biol 242:314–328. doi:10.1016/j.jtbi.2006.02.021

Ou Y, Kim DH, Kim P, Kim MJ, Julius AA (2012) Motion control of magnetized Tetrahymena pyriformis cells by magnetic field with Model Predictive Control. Int J Robot Res. doi:10.1177/0278364912464669

Peyer KE, Tottori S, Qiu F, Zhang L, Nelson BJ (2012a) Magnetic helical micromachines. Chem A Eur J 19: 28–38. doi:10.1002/chem.201203364

Peyer KE, Zhang L, Nelson BJ (2012b) Bio-inspired magnetic swimming microrobots for biomedical applications. Nanoscale. doi:10.1039/c2nr32554c

Tottori S, Zhang L, Qiu F, Krawczyk KK, Franco-Obregón A, Nelson BJ (2012) Magnetic helical micromachines: fabrication, controlled swimming, and cargo transport. Adv Mater 24:811–816. doi:10.1002/adma.201103818

Weibel DB, Garstecki P, Ryan D, DiLuzio WR, Mayer M, Seto JE, Whitesides GM (2005) Microoxen: microorganisms to move microscale loads. Proc Natl Acad Sci USA 102:11963–11967. doi:10.1073/pnas.0505481102

Zhang L, Abbott JJ, Dong L, Kratochvil BE, Bell D, Nelson BJ (2009) Artificial bacterial flagella: fabrication and magnetic control. Appl Phys Lett 94:064107. doi:10.1063/1.3079655

Zhang L, Peyer KE, Nelson BJ (2010) Artificial bacterial flagella for micromanipulation. Lab Chip 10:2203–2215

Zhang L, Petit T, Peyer KE, Nelson BJ (2012) Targeted cargo delivery using a rotating nickel nanowire. Nanomedicine: nanotechnology. Biol Med 8:1074–1080